

The High Energy Emission of the Crab Nebula from 20 keV to 6 MeV with *INTEGRAL* SPI ¹

E. Jourdain and J. P. Roques

CESR, Université de Toulouse [UPS] and CNRS, UMR 5187, 9 Av. du Colonel Roche, BP 44346, 31028 Toulouse Cedex 4, France

Received ; accepted

ABSTRACT

The SPI spectrometer aboard the INTEGRAL mission observes regularly the Crab Nebula since 2003. We report on observations distributed over 5.5 years and investigate the variability of the intensity and spectral shape of this remarkable source in the hard X-rays domain up to a few MeV. While single power law models give a good description in the X-ray domain (mean photon index ~ 2.05) and MeV domain (photon index ~ 2.23), crucial information are contained in the evolution of the slope with energy between these two values. This study has been carried out through individual observations and long duration (~ 400 ks) averaged spectra. The stability of the emission is remarkable and excludes a single power law model. The slopes measured below and above 100 keV agree perfectly with the last values reported in the X-ray and MeV regions respectively, but without indication of a localized break point. This suggests a gradual softening in the emission around 100 keV and thus a continuous evolution rather than an actual change in the mechanism parameters. In the MeV region, no significant deviation from the proposed power law model is visible up to 5-6 MeV.

Finally, we take advantage of the spectroscopic capability of the instrument to seek for previously reported spectral features in the covered energy range with negative results for any significant cyclotron or annihilation emission on 400 ks timescales.

Beyond the scientific results, the performance and reliability of the SPI instrument is explicitly demonstrated, with some details about the most appropriate analysis method.

Subject headings: supernova remnant – ISM: individual (Crab Nebula) — gamma rays: observations

1. Introduction

The Crab is a major source for the high energy domain, where it represents one of the brightest and uniquely stable source. At least two spectral components have to be considered in the observed emission, one from the pulsar itself and one from its surrounding nebula. It has been shown (Kuiper et al., 2001) that at least up to 1 MeV, the pulsed emission is harder than the nebula (non pulsed) one and that its importance grows with energy, from a few % around 1 keV to 20-30 % around 1 MeV. While both spectra can be roughly described by a power law, its slope changes with energy (broken power law). In this highly magnetized environment, the main photon production mechanism is synchrotron radiation by charged particles, with Compton collisions which scatter primary photons in the very high energy domain ($E \sim 1$ GeV). The emitted spectrum reflects thus simultaneously the distribution(s) of the charged particles and the geometry of the magnetic field.

A review of the main historical observations in X- and γ -rays can be found in Ling and Wheaton (2003). These authors present the results obtained by the *CGRO* BATSE instrument in the 30 keV-1.7 MeV energy band. The 1-2 weeks averaged spectra can be described by a variable broken power law with average photon indices of ~ 2.1 and ~ 2.4 respectively below and above an energy break close to 100 keV. Moreover, a hardening above 670 keV is proposed to be potentially related to an additional component observed in the first *CGRO* COMPTEL channels up to 3 MeV.

The analysis presented here is based on *INTEGRAL* SPI data in the 20 keV - 8 MeV energy band. The main characteristics of the SPI telescope are the spectroscopic capability of the germanium detectors and the good sensitivity achieved over more than 2 decades in energy with a unique instrument. Since the Crab has not been used as a standard candle to adjust SPI energy transfert matrix, SPI is an ideal tool to perform a robust study of the emission of this source. Our goal is to investigate the overall shape of the hard X-ray emission as well as the presence of potential spectral features linked to annihilation and cyclotron processes, since these points remain open in spite of numerous observations.

¹Based on observations with INTEGRAL, an ESA project with instruments and science data centre funded by ESA member states (especially the PI countries: Denmark, France, Germany, Italy, Spain, and Switzerland), Czech Republic and Poland with participation of Russia and USA.

2. Instrument and Observations

The INTEGRAL (INTErnational Gamma-Ray Astrophysics Laboratory) observatory is an ESA mission launched in 2002, October 17. One of its 2 main instruments is the spectrometer, SPI (Vedrenne et al., 2003), which consists of an array of 19 high purity Germanium (Ge) detectors, with a geometrical surface area of 508 cm² and a thickness of 7 cm. The detector plane temperature is maintained at ~ 80 K to reach an energy resolution between 2 and 8 keV from 20 keV to 8 MeV. The association of a coded mask together with the germanium crystals leads to an angular resolution of 2.6° (FWHM) over a 30° field of view. A 5-cm thick BGO shield (ACS, Anti-Coincidence Shield) protects the telescope from charged particles and photons originating outside the field of view. The first instrument in-flight performance is given in Roques et al. (2003).

Usually, each 3-day orbit is filled with roughly one hundred of exposures lasting 30-40 minutes. During an observation dedicated to a given source, the pointing direction varies around the target by steps of $\sim 2^\circ$ within a 5×5 square or a 7-point hexagonal pattern. This dithering procedure (see Jensen et al., 2003, for details) is used to optimize the imaging capabilities of both IBIS (the second main INTEGRAL instrument) and SPI. This approach is crucial for SPI since it increases the number of measurements (equal, for one exposure, to the number of detectors, see equation (1)) on a same sky region, eliminating ghost images and permitting a robust background and source fluxes estimation.

2.1. Instrument Management

The SPI telescope has been carefully calibrated before its launch (Attié et al., 2003), ranging from individual calibration up to full instrument calibrations. Each step has been reproduced and compared to Monte-Carlo simulations. This provides confidence in the simulation tools and in our understanding of the instrument. The simulation tool has then been used to construct the response matrix. This matrix has been split in two parts, one reflecting the geometry (ray tracing), the other taking into account the energy redistribution (Sturmer et al., 2003). The information has been put in IRF and RMF files respectively, for 51 energy values and 95 angles in both directions. Specific interpolation subroutines allow to recover the information for any value of energy and incident direction.

Due to 2 detector failures, the 1st one (detector N°2) during revolution 140 (December 6th, 2003), the second one (detector N°17) after revolution 214 (July 17th, 2004), SPI data have to be analysed with background fields and IRF matrices according to the detector plane configuration (spi_irf_grp_0021.fits, spi_irf_grp_0022.fits, spi_irf_grp_0023.fits, for 19, 18 or 17

detectors, respectively, the RMF information being unaffected). Moreover, data will be added only within periods corresponding to the same configuration.

Note that a 3rd failure (detector N°5) occurred on 2009, 19 February, after the last revolution considered in the present analysis.

The excellent energy resolution of the germanium crystals makes it crucial to determine very accurately the channel-energy relation for each detector and each revolution to ensure reliable results for spectral studies.

For the low energy chain (0-2 MeV), we use 6 background lines between 23.438 keV and 1763.367 MeV to build an energy-channel relation, $E=f(c)$, through a function of the form:

$$E(c) = A0 \times Ln(c) + A1 + A2 \times c + A3 \times c^2 + A4 \times c^3$$

where the five free parameters $(Ai)_{i=0,4}$, are adjusted for each detector and each revolution.

For the high energy chain (2-8 MeV), a simple linear relation based on 2 lines (2754.028 and 7415.60 keV) was used (2 free parameters).

Second order drifts due to dependence on the detectors temperature on a few hours timescale have not been included. This can result in small discontinuities in the final spectra at the edge of strong background lines, but doesn't influence the final scientific conclusions.

A second issue has been investigated in order to use data above 1 MeV. There, the energy output of the electronic chain is contaminated by high energy particles, which saturate the electronic and generate false triggers around 1.4 MeV (see SPI team document by Wunderer, 2005). Fortunately, a second electronic chain ("PSD") operates in parallel from the fast preamplifier output and generates an independent trigger for photon energies between 650 keV and 2.2 MeV. The "PSD" electronic box (originally designed to perform Pulse Shape Discrimination) has an efficiency of 85% on its global energy domain due to a higher dead time but is not affected by the saturation problem. We thus use the trigger signal issued from the PSD electronic to confirm the reality of the events between 650 keV and 2.2 MeV and complete a clean analysis in the whole energy range covered by our instrument (20 keV-8 MeV). We have consequently built background patterns identically formed with "PSD" tagged events only, in the corresponding energy range. The appropriate factor (0.85) is applied to the data and error bars to take into account the additional dead time related to PSD event selection.

2.2. Data Set

Crab is used as a reference target to monitor or calibrate instruments. During the INTEGRAL mission, regular campaigns to measure Crab are planned, (roughly twice a year). Since these observations are carried out mainly for performance monitoring or calibration

purposes, various exotic pointing schemes have been realized. To ensure results as robust as possible, we restricted our set of data to the standard dithering patterns, optimized for the SPI telescope observations. We have analysed 13 observations dedicated to this source from 2003, February 19th to 2008 September 28th, corresponding to 10 periods generally spaced by ~ 6 monthes (see Table 1). After data analysis and cleaning, we obtained 1.2×10^6 seconds of effective observing time.

The stability of the instrument (within 5%) has been checked over the mission timescale (Jourdain & Roques, 2009), making us confident to sum data to obtain better signal to noise ratio. We have conducted our analysis by first analysing individual revolutions, and then building 3 long duration averaged spectra for 3 periods (see Table 1) :

Sum 1 corresponds to the beginning of the mission (19 detectors alive) with 3 revolutions and 402 ks of useful duration.

Sum 2 groups 7 observations (of 30 to 70 ks each) spaced by 6 monthes from 2004 September to 2007 September for a total useful duration of 325 ks (17 detectors alive).

Sum 3 corresponds to a specific long campaign dedicated to the Crab, performed in March and September 2008, with 3 entire revolutions for 462 ks (17 detectors alive).

2.3. Analysis Method

The flux extraction in the count space is based on a model fitting algorithm using χ^2 minimization, with a sky model consisting of N_s sources at their theoretical positions. For a given energy bin, E , the SPI data, integrated during a time interval (or pointing) p , can be expressed with the general formula:

$$D_p = \sum_{i=1}^{N_s} M_{p,i} \times S_{p,i} + B_p \quad (1)$$

Where D , M , B are N_d elements vectors (one element per detector, $N_d = 19, 18$ or 17), and represent respectively:

$D_p(E)$: data (number of counts) measured on the detector plane for the pointing p .

$S_{p,i}(E)$: intensity of source i , during the pointing p .

$M_{p,i}(E)$: SPI spatial/geometrical response (IRF) for the source i for the direction of pointing p .

$B_p(E)$: background counts measured on the detector plane for the pointing p .

For the Crab observations, the sky model contains only this source, since the contri-

bution of any other source can be considered as negligible (i.e. A0535+262 doesnot exceed 15 mCrab during the considered periods). Nevertheless, this system is solvable only if some external (a priori) information is introduced.

The main information we can introduce concerns the background component. From empty field observations, the relative factors between detectors, $U[d]$, are measured to describe the background maps on the detector plane . For each energy band, B_p in equation (1) is thus reduced to $\beta(p)*U[d]$, with only one free parameter per pointing, the global normalisation factor $\beta(p)$ of a fixed vector, d being the detector number.

We thus consider a set of N_p equations to treat simultaneously N_p pointings. The variability of the background intensity, $\beta(p)$, can be constrained, since it is not expected to vary on the pointing (~ 2 ks) timescale. By looking at the count rates measured in the anti-coincidence system, it can be seen that the background intensity is in general stable on the orbit (3 days) timescale. The spectra have thus been built with the background normalisation $\beta(p)$ allowed to vary on the revolution timescale (~ 2.5 days) while the source is considered as constant. Consequently, for an observational period encompassing N_p pointings and N_r revolutions, the number of free parameters is N_r (background intensities) + 1 (the Crab intensity), while the number of data is N_p*N_d (with $N_p \sim 10 - 100N_r$).

At the end of the flux extraction procedure, χ^2 for individual energy channels are checked to detect any problems. Except at low energy where the high level of statistic surpasses our instrument knowledge precision (with source detection levels greater than 100σ), all χ^2 values are acceptable.

At this stage, a count spectrum and its associated response matrix (i.e. for the Crab nebula position and a given pointing sequence) are stored.

3. Spectral Analysis

From the count spectra and the corresponding matrices, we have reconstructed the incident photon spectra through a spectral fitting procedure (Xspec11 tools).

Some non-statistical features appear in the lower channels due to the uncertainties on the energy response, which drops off dramatically in this domain, and threshold effects. We have thus excluded the first channels ($E < 23.5$ keV) from the fit process. No systematic has been introduced in order to keep data as free as possible of any subjective information.

3.1. Analysis of individual observations

Considering the 13 observations presented in Table 1, the spectral variability of the Crab emission has been investigated at two levels:

- The potential evolution of the spectral shape in terms of one or two slopes model, as observed by BATSE (Ling & Wheaton, 2003)
- The stability of the parameters of the powerlaw(s).

The fits have been performed on 79 logarithmic channels between 23.5 keV and 1 MeV, with single power law and broken power law models. In all cases, the 2 slopes model provides a significant improvement in the χ^2 value when compared to a single power law. However, a degeneracy between the break energy and the slopes (the low energy one essentially) prevents us from constraining clearly the parameters. Indeed, a gradual steepening of the spectral emission toward high energies is probably closer to the reality than the broken power law model. This pushed us to test the parameters variability through a broken powerlaw model with the energy break fixed to 100 keV. This specific energy break has been chosen because it allows easy comparisons with other observational results and is very close to the values reported from BATSE data (Ling & Wheaton, 2003).

The fitted photon index values are displayed in Table 1. They are all compatible with photon indices of 2.07 and 2.24 below and above 100 keV respectively, demonstrating a remarkable stability of the spectral shape emission between 23 keV and 1 MeV, even though this analytical law doesn't represent a physical mechanism.

An important point, for comparison with other data sets, is the spectrum normalisation. The 100 keV flux in the last column of Table 1 is the normalisation given by the broken powerlaw model, with energy break fixed to 100 keV. To obtain a model independent flux, we have made a local (82-118 keV) fit with a power law model, and obtained systematically lower values but always strikingly stable. (see Column 5 of Table 1).

3.2. Analysis of long duration averaged spectra

The three summed spectra encompassing more than 300 ks allow us to better constrain the spectral shape, over an energy domain extended up to 6 MeV (7 channels more). The broken power law model with the break energy fixed to 100 keV gives the same indices than for the individual spectra, but we can try to learn more by letting free the break energy. A simultaneous fit of the three spectra converges toward photons indices of 2.04 and 2.18, respectively below and above a break energy of 62 keV. Figure 1 displays the 3

averaged spectra together with this broken power law fit. However, it is clear that these values are strongly drawn by the low energy high signal to noise ratio. When adding some systematics to the data, we observe that the fitted energy break increases with the value of the systematic, with correlated changes in the fitted slopes. For example, a reasonable value of 1% of systematic ends up in a "banana" 90% confidence region from 70 to 90 keV for the energy break, and from 2.05 to 2.08 for the first slope, the second one remaining above 2.18. In fact, we can see it as a region of more or less equivalent solutions, since we stress again that such a 2 slope model is an analytical description of a probably smooth evolution. This can be illustrated by using a formula where the slope is continuously varying with $\text{Log}(E)$ as proposed by Massaro et al. (2000)

$$F(E) = A \times E^{a+b\text{Log}(E/E_0)}$$

A simultaneous fit of the three spectra gives

$$a=1.79 \pm 0.02$$

$$b=0.134 \pm 0.01$$

$$A= 3.87 \text{ ph cm}^{-2} \text{ s}^{-1} \text{ keV}^{-1}$$

with E_0 fixed to 20 keV.

We then get $\chi = 421$ for 253 dof, clearly better than $\chi = 453$ for 252 dof obtained for the broken powerlaw model. To provide complete information, fluxes and errors of the three spectra are given in Table 2.

Note that the continuous curvature prevents any safe extrapolation outside the considered energy range while representing very well the SPI data.

4. Discussion

The hard X-ray domain is important for the study of the Crab Nebula emission since it joins the X-ray band where a photon index of ~ 2 -2.1 is known from many measurements to the MeV and above domain where observations are much rarer but indicate an increase of the photon index (2.2-2.3). The shape of this spectral evolution contains information on the main parameters of the emission itself, magnetic field value and charged particles distribution. The disagreement between the most recent results limits any firm conclusion: While the spectrum measured by the PDS instrument (15-300 keV; Kuiper et al. 2001) aboard the BeppoSAX mission is compatible with a single slope power law model (photon index of 2.14) found by the GRIS balloon experiment (20-700 keV; Bartlett et al. 1994), the detailed analysis performed by Ling & Wheaton (2003) with the BATSE data (35 keV-1

MeV) concludes that the ~ 10 days averaged spectra are better described with a slope varying from 2.1 to 2.4 around a break at ~ 100 keV. Moreover, these authors report a hardening above ~ 700 keV, which could be an additional structure superimposed to the powerlaw component.

From the analyses based on a large set of SPI data, we confirm the first finding of BATSE, namely the slope softening in the hard X-ray emission of the total spectrum. Our results show a quite satisfying agreement with the BATSE ones as the two slopes and energy break values can be considered as the same. Moreover, the 40 keV fluxes are quite similar (4.5×10^{-3} ph cm $^{-2}$ s $^{-1}$ keV $^{-1}$ for BATSE to compare to $4.4 \pm 0.1 \times 10^{-3}$ ph cm $^{-2}$ s $^{-1}$ keV $^{-1}$ obtained from SPI data). However, we can not confirm the variability observed on a 10 days timescale nor the emission in excess of the powerlaw observed above 700 keV (see section 4.2).

4.1. Comparison with X-ray results

The X-ray slope (above 1.5 keV to avoid absorption effects) has a standard value of 2.1 but recent study with XMM data (Kirsch et al. 2006) reports a value of 2.046 for the total (nebula + pulsar) spectrum. This "mean" slope summarizes in fact strong variations of the photon index inside the nebula structure (from 2.0 to 2.4) and during the phase of the pulsed emission (from 1.5 to 1.75), which are similarly contained in our total spectrum. The agreement between the slope we have obtained in the low energy part of SPI spectra and this mean X-ray value confirms that the same mechanisms underlie the emission from soft to hard X-rays.

Concerning the spatial variations of the emission (very well studied below 10 keV), a first result from a balloon-borne telescope in the 22-64 keV energy range (Pelling et al. 1987) points out the interest of spatially resolved (below 30") data in the hard X-ray domain for future instruments. It is the only way to access the topological information and to link a particular region with the macroscopic parameters deduced from observations (magnetic field value, for example).

4.2. Comparison with results at higher energy

The main observations for comparing our results in the MeV region have been performed with COMPTEL. Kuiper et al. (2001) present a complete analysis of pulsed and non pulsed emission. They report a clear evolution of the pulse morphology explained by a three-component model, with fraction of pulsed over non pulsed emission presenting a maximum

($\sim 30\%$) around 1 MeV.

The high energy slope deduced from SPI data (2.24 ± 0.04) is quite consistent with the values deduced from COMPTEL data (photon index of 2.35 for the pulsed emission, 2.23 for the nebula). However, while it implies a pronounced break around 1 MeV in the pulsed emission (see Kuiper et al, 2001), it corresponds to a more continuous curvature of the nebula spectral emission, pointing out noticeable differences in the emitting processes. However, in this region, the total emission as measured by SPI does not exhibit any particular feature. More precisely, the hardening observed above 700 keV in the BATSE data and possibly related to some similar structure in the first COMPTEL channels cannot be confirmed. Figure 2 shows the high energy part of our 3 averaged spectra. No deviation from the high energy power law can be observed while the flux remains unchanged within errors. Slightly positive residuals are present above 2-3 MeV, but well above the BATSE excess and their significance is too low to reject a statistical nature.

4.3. Search for annihilation and cyclotron features

The excellent energy resolution of the SPI detector plane makes it the best instrument to seek for (narrow) spectral features in the observed emission. Concerning the Crab Nebula, several detections have been reported of two different natures, attributed to cyclotron emission in one hand, at $E \sim 75$ keV, and to annihilation in the other hand, around 400 keV and above (see Owens (1991) for a summary). For the cyclotron emission, detections correspond to fluxes between 0.3 and 1×10^{-2} ph cm $^{-2}$ s $^{-1}$ while the most constraining 3σ upper limit is 6.2×10^{-4} ph cm $^{-2}$ s $^{-1}$. As regard the "annihilation" mechanism, photon production varies between 1×10^{-4} ph cm $^{-2}$ s $^{-1}$ and 7.2×10^{-3} ph cm $^{-2}$ s $^{-1}$. Variabilities (in energy, flux and possibly phase region) point out the complexity of the physics contained in the Crab emission.

We have looked for the presence of similar structures in the SPI data by re-building spectra with 5 keV width channels. In each averaged spectrum, no significant excess has been found, in the mentioned energy domains. Considering the summed spectra, this leads to 4σ upper limits of 2×10^{-4} ph cm $^{-2}$ s $^{-1}$ in a 5 keV width band, around 75 keV while they are between 1.5 and 2×10^{-4} ph cm $^{-2}$ s $^{-1}$ for a 3σ significance in the 400-600 keV domain. Concerning a broader feature, upper limit values are between 2 and 3.3×10^{-4} ph cm $^{-2}$ s $^{-1}$ for a 25 keV band centered on 511 keV, for the accumulated spectra.

In conclusion, no feature corresponding to cyclotron or annihilation emission on timescales of 400 ks has been detected, for the total Crab emission.

5. Conclusions

We have used the *INTEGRAL* SPI data to study the spectral emission of the Crab from 20 keV to a few MeV. As preliminary remarks, it is worth to mention that the SPI telescope benefits from an "absolute" calibration, in the sense that its transfert matrices are based on ground calibrations and Monte-Carlo simulations, and therefore independent from Crab observations, which are often used for calibrations of other X-and γ -ray instruments. Moreover, details on some analysis aspects which require particularly careful handling are explicated .

Beyond the good agreement of our results with previous works, particularly with the analysis of BATSE data by Ling & Wheaton (2003), we point out the impressive stability of the total Crab emission from 20 keV to a few MeV. The spectral parameters have been found very stable on the 6 years timescale and rule out a single powerlaw model. Broken power law models give a good description of the SPI data even though the energy break cannot be firmly constrained, probably because the transition from the low energy slope to the high energy one is smooth.

Three mean spectra have been built in order to achieve a better statistic (total useful duration of ~ 400 ks) and investigate deeply the spectral shape, including the MeV region. Using a broken power law model, the best fit procedure converges toward slope values of 2.07 ± 0.01 and 2.23 ± 0.05 for a break fixed at 100 keV. When letting free the energy break, the fit procedure converges toward a value of 62 keV, while the power-law indices become 2.04 and 2.18 respectively. These values are close to those reported from instruments in adjacent energy bands, pointing out a coherent view of the wide band emission.

Another important result is the continuous curvature in the 100 keV region, we can describe by the analytical law

$$F(E) = 3.87 \times E^{1.79+0.134\text{Log}(E/20)} \text{ ph cm}^{-2} \text{ s}^{-1} \text{ keV}^{-1} \quad (2)$$

valid in the 23 keV-6 MeV domain, with E expressed in keV .

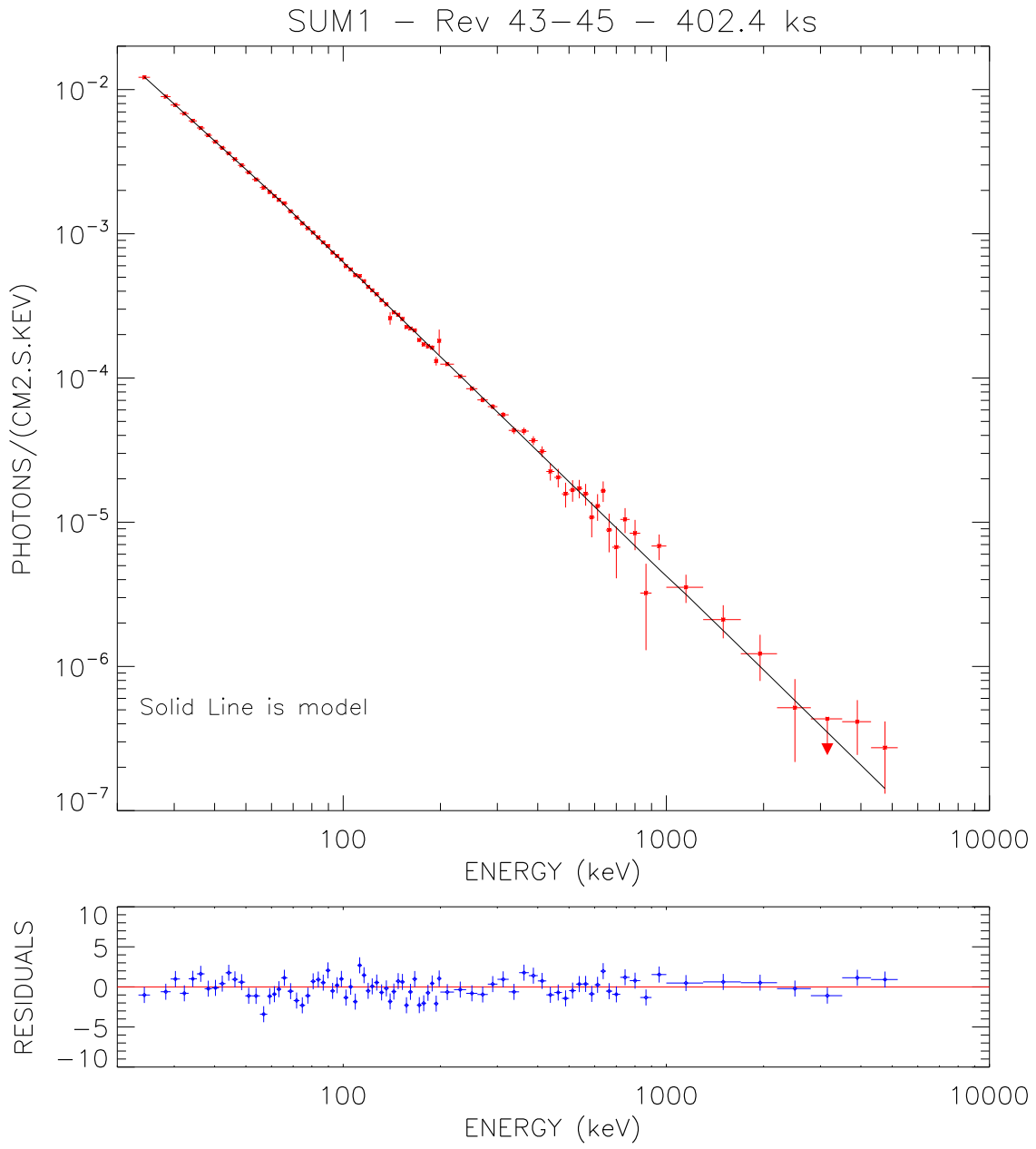
This gradual steepening provides information about the acceleration mechanism(s) and charged particle distributions participating to the X/ γ -ray production and gives opportunities to test models and learn more about emission parameters. However, the pulsed/non-pulsed fraction as well as the spatial distribution have to be investigated in more details in order to better understand the global nebula emission in hard X-rays. All these ingredients plays a crucial role in the global/averaged shape observed in this domain and have be considered in the model in order to explain the observed spectral emission.

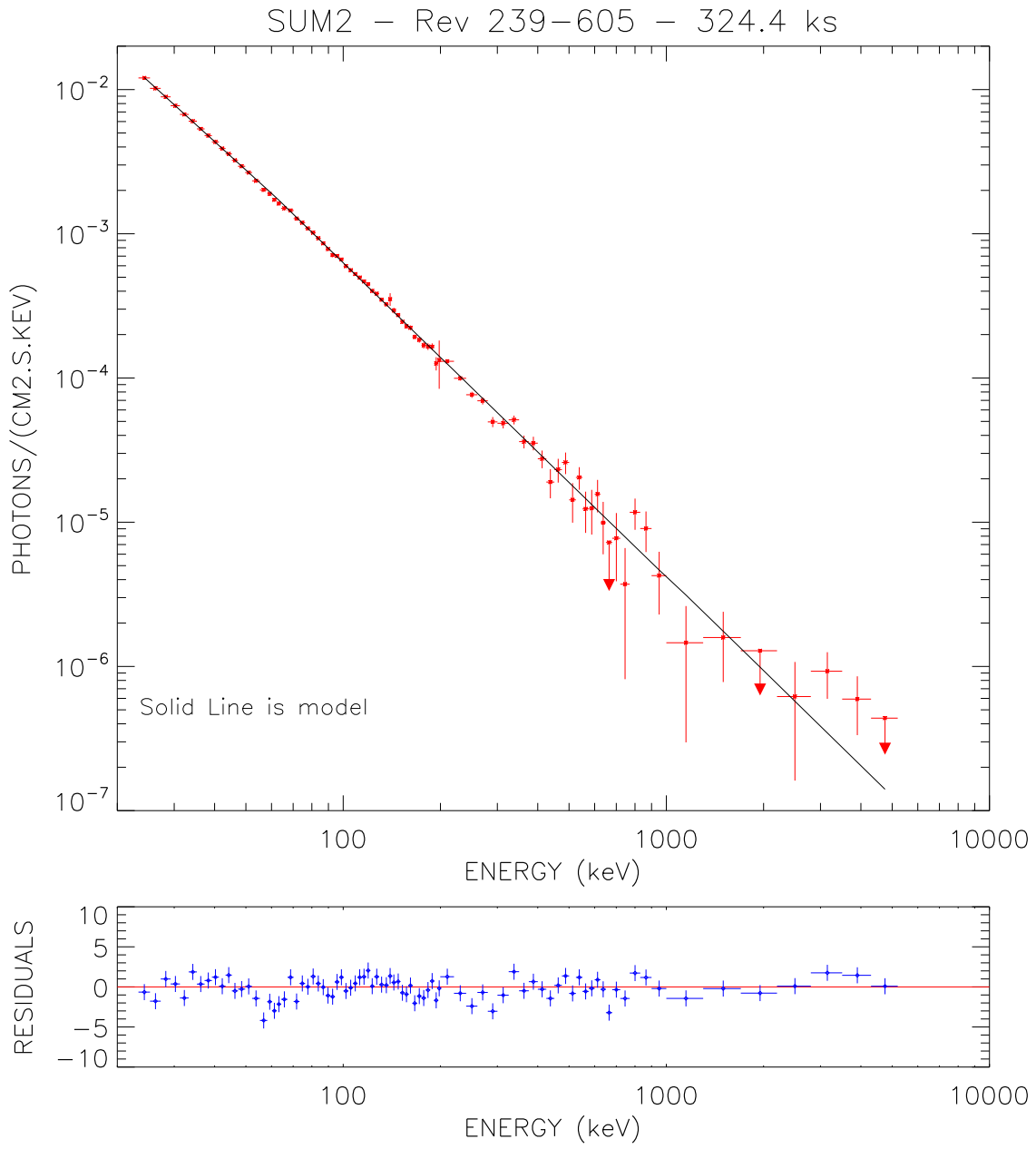
Acknowledgments

The *INTEGRAL* SPI project has been completed under the responsibility and leadership of CNES. We are grateful to ASI, CEA, CNES, DLR, ESA, INTA, NASA and OSTC for support.

REFERENCES

- Attié D., Cordier B., Gros M., et al, 2003, *A&A*, 411, L71
- Bartlett L. M., Barthelmy S. D., Gehrels N., Teegarden B. J., Tueller J., Leventhal M. and MacCallum C. J., 1994, in *The Second Compton Symp.*, College park MD, 1993, Ed. C. E. Fichtel, N. Gehrels & J. P. Norris, *AIP conf. Proc.*, 304, 67
- Jensen, P.L., Clausen, K., Cassi, C. et al., 2003, *A&A*, 411, L7
- Jourdain, E. & Roques, J. P., 2009, *Proceedings of the 7th INTEGRAL workshop*, September 2008, Copenhagen, PoS(Integral08)143, astro-ph0809.5018
- Kirsch M. G. F., Schönherr G., Kendziorra E. et al., 2006, *A&A*, 453, 173
- Kuiper, L., Hermsen, W. , Cusumano, G., Dielh, R., Schönfelder, V., Strong., A., Bennett, K. and McConnell, M. L., 2001, *A&A*, 378, 918
- Ling, J. C.& Wheaton, WM. A., 2003, *ApJ*, 598, 334
- Massaro, E., Cusumano, G., Litterio, M. and Mineo, T., 2000, *A&A*, 361, 895
- Owens, A., 1991, *AIP conf. Proc.* 232, *Gamma-Ray Line Astrophysics*, Ed. PH. Durouchoux & N. Prantzos (Paris-Saclay), 341
- Pelling, R. M., Paciesas, W. S., Peterson, L. E., Makishima, K., Oda, M., Ogawara, Y., Miyamoto, S 1987, *ApJ*, 319, 416
- Roques J.P., Schanne S., Von Kienlin A., et al, 2003, *A&A*, 411, L91
- Sturner S.J., Shrader C. R., Weidenspointner G., et al, 2003, *A&A*, 411, L81
- Vedrenne, G., Roques, J.P., Schonfelder, V. et al, 2003, *A&A*, 411, L63
- Wunderer, T., SPI Scientific Team Meeting, R Roma - March 17, 2005, http://sigma-2.cesr.fr/spi/download/docs/4303-CR_SPI-CoIs_March17.pdf, p.71





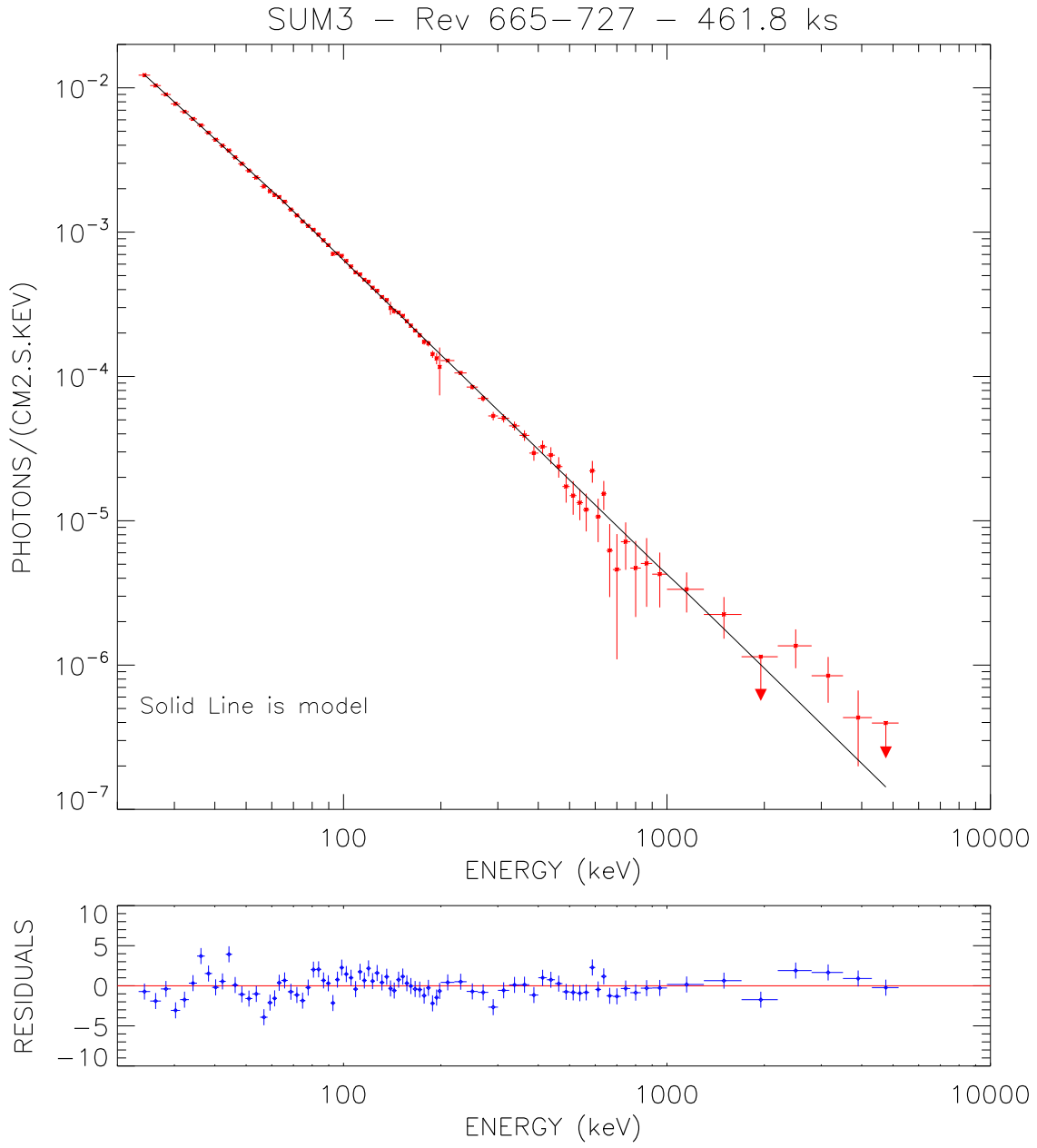


Fig. 1. Grab averaged spectra for the three epochs (sum1, sum2, sum3, see Tab. 1). Solid

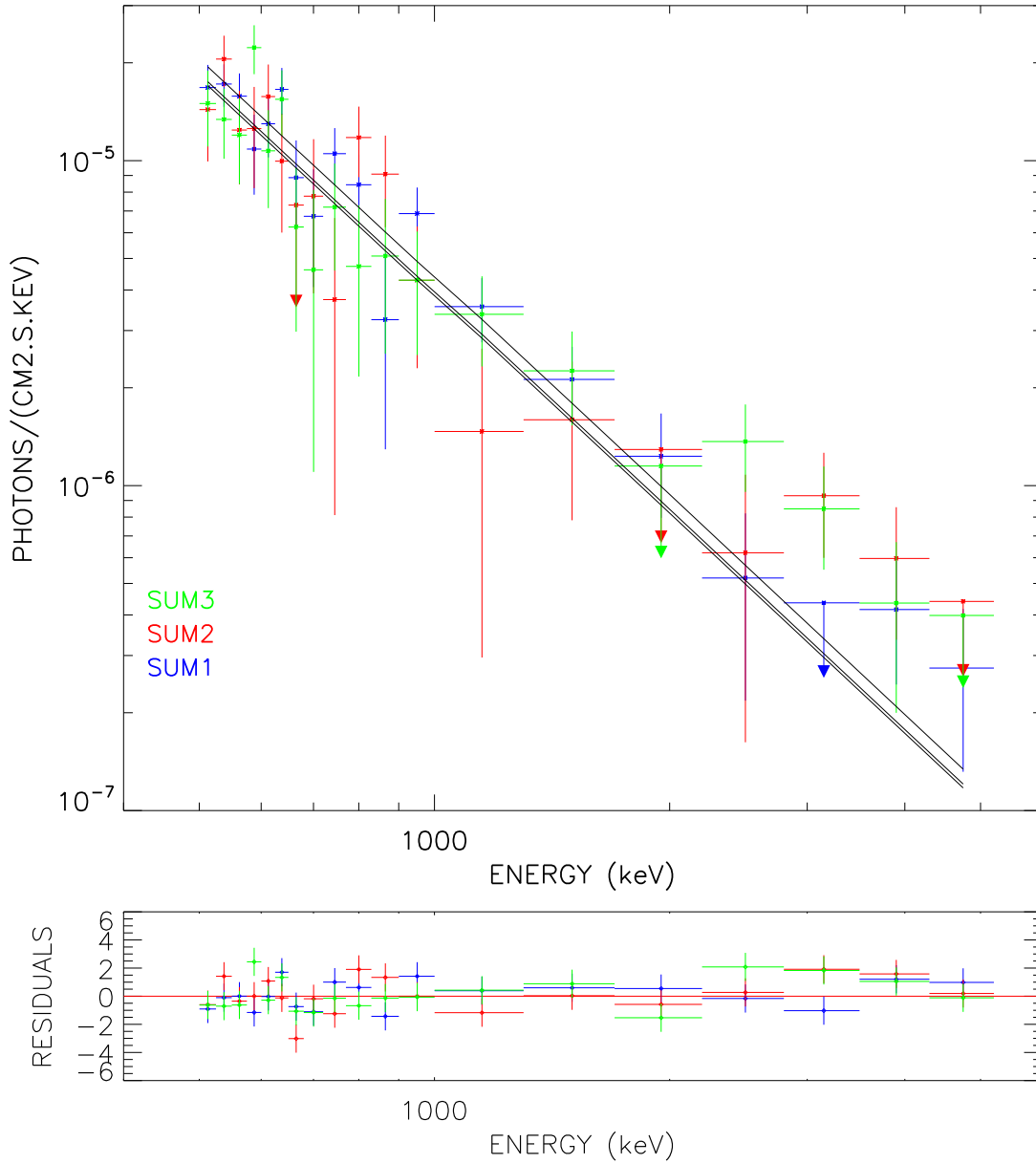


Fig. 2 Crab spectra for three epochs (sum1, sum2, sum2) above 500 keV; Solid lines

Table 1. Log of the *INTEGRAL* SPI observations dedicated to the Crab used in this paper (standard dithering modes).

revol number	Start	End	useful duration ks	F_{100keV} $\times 10^{-4} ph /$ $cm^2 s keV$	<i>index1</i>	<i>index2</i>	F_{100keV} $\times 10^{-4} ph /$ $cm^2 s keV$
43	2003-02-19 16:06:05	2003-02-21 15:59:22	139.94	6.3 ± 0.2	2.08 ± 0.01	2.25 ± 0.03	6.5 ± 0.2
44	2003-02-22 04:06:15	2003-02-24 12:10:57	156.22	6.5 ± 0.2	2.07 ± 0.01	2.24 ± 0.03	6.6 ± 0.2
45	2003-02-25 03:58:54	2003-02-26 16:51:08	106.22	6.5 ± 0.2	2.05 ± 0.01	2.24 ± 0.03	6.8 ± 0.2
Sum 1	rev 43	rev 45	402.38	6.45 ± 0.1	2.07 ± 0.01	2.24 ± 0.02	6.6 ± 0.1
239	2004-09-29 11:12:34	2004-09-29 22:38:05	31.14	6.4 ± 0.2	2.07 ± 0.02	2.33 ± 0.07	6.6 ± 0.2
300	2005-03-29 12:00:27	2005-03-30 01:18:30	38.72	6.3 ± 0.2	2.08 ± 0.02	2.23 ± 0.07	6.5 ± 0.2
365	2005-10-11 08:33:49	2005-10-11 19:11:44	30.51	6.6 ± 0.2	2.05 ± 0.02	2.31 ± 0.07	6.8 ± 0.2
422	2006-03-28 17:28:11	2006-03-29 07:27:19	38.70	6.5 ± 0.2	2.07 ± 0.0	2.23 ± 0.07	6.6 ± 0.2
483*	2006-09-29 01:40:14	2006-09-29 14:27:34	32.41	6.5 ± 0.3	2.1 ± 0.03	2.26 ± 0.08	6.5 ± 0.2
541	2007-03-19 13:25:14	2007-03-20 15:34:16	71.34	6.3 ± 0.2	2.07 ± 0.02	2.27 ± 0.08	6.4 ± 0.2
605	2007-09-27 00:21:34	2007-09-28 06:09:51	81.56	6.4 ± 0.2	2.07 ± 0.02	2.24 ± 0.05	6.6 ± 0.2
Sum 2	Rev 239	Rev 605	324.4	6.35 ± 0.1	2.07 ± 0.01	2.25 ± 0.03	6.55 ± 0.1
665	2008-03-24 11:57:5	2008-03-27 00:06:30	146.44	6.6 ± 0.2	2.07 ± 0.01	2.27 ± 0.03	6.7 ± 0.2
666	2008-03-27 11:40:28	2008-03-29 23:51:34	154.35	6.5 ± 0.2	2.06 ± 0.01	2.26 ± 0.03	6.7 ± 0.2
727	2008-09-25 22:34:01	2008-09-28 11:06:32	161.02	6.5 ± 0.2	2.07 ± 0.01	2.22 ± 0.03	6.7 ± 0.2
Sum 3	Rev 665	Rev 727	461.81	6.5 ± 0.1	2.06 ± 0.01	2.25 ± 0.04	6.7 ± 0.1

Note. — Columns 6 to 8 give the best fit parameters for a broken power law model with the break energy fixed to 100 keV. The data have been fitted between 23.5 and 1 MeV (6 MeV for summed spectra) with no systematic. Column 5 is the model independent 100 keV flux (see section 3.1).

* Rev 483 has been performed with a 5x5 grid with 1° degree step instead of 2°.

Table 2. Fluxes and errors for the three Crab spectra (sum1, sum2 and sum3) in the energy channels used in this analysis. The deconvolution is based on the powerlaw with energy dependent slope model (equation (2)). Fluxes and errors are given in units of $ph / cm^2 s keV$

E_{min}	E_{max}	Flux (sum1)	error (sum1)	Flux (sum2)	error (sum2)	Flux (sum3)	error (sum3)
23.25	25.25	1.22E-02	7.17E-05	1.20E-02	1.06E-04	1.22E-02	9.40E-05
25.25	27.25	1.02E-02	4.25E-05	1.02E-02	6.06E-05	1.04E-02	5.32E-05
27.25	29.25	8.94E-03	2.90E-05	8.91E-03	4.06E-05	8.99E-03	3.54E-05
29.25	31.25	7.81E-03	2.52E-05	7.72E-03	3.48E-05	7.74E-03	3.02E-05
31.25	33.25	6.82E-03	2.24E-05	6.72E-03	3.06E-05	6.83E-03	2.66E-05
33.25	35.25	6.07E-03	2.02E-05	6.04E-03	2.77E-05	6.09E-03	2.40E-05
35.25	37.25	5.42E-03	1.87E-05	5.34E-03	2.55E-05	5.50E-03	2.21E-05
37.25	39.25	4.82E-03	1.74E-05	4.80E-03	2.37E-05	4.89E-03	2.06E-05
39.25	41.25	4.35E-03	1.63E-05	4.33E-03	2.23E-05	4.37E-03	1.95E-05
41.25	43.25	3.95E-03	1.56E-05	3.90E-03	2.14E-05	3.97E-03	1.87E-05
43.25	45.25	3.61E-03	1.50E-05	3.58E-03	2.08E-05	3.68E-03	1.83E-05
45.25	47.25	3.29E-03	1.51E-05	3.23E-03	2.09E-05	3.30E-03	1.83E-05
47.25	49.75	2.98E-03	1.29E-05	2.94E-03	1.83E-05	2.98E-03	1.62E-05
49.75	52.25	2.67E-03	1.47E-05	2.66E-03	2.16E-05	2.67E-03	1.92E-05
52.25	55.25	2.38E-03	2.93E-05	2.33E-03	4.12E-05	2.39E-03	3.59E-05
55.25	58.25	2.09E-03	2.02E-05	2.02E-03	2.90E-05	2.07E-03	2.56E-05
58.25	60.25	1.95E-03	2.54E-05	1.89E-03	3.61E-05	1.92E-03	3.17E-05
60.25	62.25	1.82E-03	2.56E-05	1.72E-03	3.66E-05	1.81E-03	3.22E-05
62.25	64.25	1.72E-03	2.91E-05	1.62E-03	4.14E-05	1.75E-03	3.63E-05
64.25	67.25	1.62E-03	3.21E-05	1.50E-03	4.50E-05	1.62E-03	3.92E-05
67.25	70.25	1.43E-03	1.47E-05	1.45E-03	2.16E-05	1.43E-03	1.93E-05
70.25	73.25	1.30E-03	9.05E-06	1.27E-03	1.32E-05	1.30E-03	1.17E-05
73.25	76.25	1.18E-03	8.81E-06	1.19E-03	1.26E-05	1.19E-03	1.11E-05
76.25	79.25	1.09E-03	8.36E-06	1.09E-03	1.19E-05	1.10E-03	1.05E-05
79.25	82.25	1.02E-03	7.61E-06	1.02E-03	1.09E-05	1.04E-03	9.66E-06
82.25	85.25	9.43E-04	7.71E-06	9.31E-04	1.11E-05	9.62E-04	9.81E-06
85.25	88.25	8.71E-04	7.89E-06	8.58E-04	1.15E-05	8.79E-04	1.02E-05
88.25	91.25	8.23E-04	8.42E-06	7.84E-04	1.24E-05	8.13E-04	1.11E-05
91.25	94.25	7.41E-04	1.79E-05	7.12E-04	2.49E-05	7.07E-04	2.18E-05
94.25	97.25	7.02E-04	1.09E-05	7.02E-04	1.58E-05	7.14E-04	1.40E-05
97.25	100.25	6.64E-04	9.57E-06	6.64E-04	1.38E-05	6.86E-04	1.22E-05
100.25	103.75	5.97E-04	9.64E-06	5.97E-04	1.37E-05	6.31E-04	1.21E-05
103.75	107.25	5.67E-04	6.39E-06	5.60E-04	9.40E-06	5.78E-04	8.38E-06
107.25	110.75	5.17E-04	6.10E-06	5.27E-04	8.99E-06	5.28E-04	7.99E-06
110.75	114.25	5.09E-04	6.07E-06	4.99E-04	8.97E-06	5.10E-04	7.97E-06
114.25	117.75	4.70E-04	6.06E-06	4.68E-04	9.01E-06	4.69E-04	8.03E-06
117.75	121.25	4.29E-04	6.59E-06	4.48E-04	9.82E-06	4.54E-04	8.73E-06
121.25	124.75	4.06E-04	6.26E-06	4.03E-04	9.67E-06	4.14E-04	8.65E-06
124.75	129.25	3.82E-04	5.47E-06	3.86E-04	8.21E-06	3.93E-04	7.34E-06
129.25	133.75	3.47E-04	5.62E-06	3.50E-04	8.54E-06	3.57E-04	7.67E-06
133.75	138.25	3.25E-04	6.87E-06	3.26E-04	1.08E-05	3.39E-04	9.78E-06
138.25	141.25	2.61E-04	2.58E-05	3.53E-04	3.57E-05	2.99E-04	3.11E-05
141.25	145.75	2.86E-04	7.73E-06	2.95E-04	1.34E-05	2.85E-04	1.22E-05
145.75	150.25	2.76E-04	5.38E-06	2.75E-04	8.22E-06	2.79E-04	7.38E-06

Table 2—Continued

E_{min}	E_{max}	Flux (sum1)	error (sum1)	Flux (sum2)	error (sum2)	Flux (sum3)	error (sum3)
150.25	154.75	2.58E-04	5.16E-06	2.47E-04	7.77E-06	2.64E-04	6.95E-06
154.75	159.25	2.27E-04	5.39E-06	2.29E-04	8.09E-06	2.43E-04	7.23E-06
159.25	163.75	2.21E-04	5.77E-06	2.24E-04	8.57E-06	2.26E-04	7.63E-06
163.75	169.25	2.15E-04	4.75E-06	1.94E-04	7.19E-06	2.09E-04	6.44E-06
169.25	174.75	1.85E-04	5.09E-06	1.85E-04	7.99E-06	1.94E-04	7.19E-06
174.75	180.25	1.72E-04	5.47E-06	1.70E-04	8.53E-06	1.75E-04	7.70E-06
180.25	185.75	1.67E-04	6.10E-06	1.66E-04	8.92E-06	1.71E-04	7.95E-06
185.75	191.25	1.63E-04	6.19E-06	1.66E-04	9.17E-06	1.44E-04	8.22E-06
191.25	196.75	1.32E-04	9.13E-06	1.27E-04	1.35E-05	1.35E-04	1.20E-05
196.75	199.75	1.82E-04	3.62E-05	1.34E-04	4.93E-05	1.17E-04	4.28E-05
199.75	220.25	1.26E-04	2.81E-06	1.32E-04	4.25E-06	1.30E-04	3.83E-06
220.25	240.25	1.04E-04	2.48E-06	1.01E-04	3.70E-06	1.07E-04	3.30E-06
240.25	260.25	8.51E-05	2.47E-06	7.74E-05	3.71E-06	8.54E-05	3.32E-06
260.25	280.25	7.11E-05	2.65E-06	7.03E-05	3.98E-06	7.13E-05	3.56E-06
280.25	300.25	6.40E-05	2.69E-06	5.02E-05	4.04E-06	5.39E-05	3.61E-06
300.25	325.25	5.61E-05	2.65E-06	4.91E-05	3.89E-06	5.20E-05	3.46E-06
325.25	350.25	4.38E-05	2.48E-06	5.19E-05	3.67E-06	4.60E-05	3.27E-06
350.25	375.25	4.33E-05	2.53E-06	3.67E-05	3.73E-06	3.95E-05	3.32E-06
375.25	400.25	3.73E-05	2.63E-06	3.58E-05	3.87E-06	2.98E-05	3.45E-06
400.25	425.25	3.13E-05	2.69E-06	2.79E-05	3.91E-06	3.30E-05	3.48E-06
425.25	450.25	2.27E-05	3.06E-06	1.93E-05	4.40E-06	2.89E-05	3.89E-06
450.25	475.25	2.07E-05	3.06E-06	2.35E-05	4.41E-06	2.41E-05	3.91E-06
475.25	500.25	1.59E-05	3.11E-06	2.64E-05	4.50E-06	1.75E-05	3.99E-06
500.25	525.25	1.69E-05	2.89E-06	1.45E-05	4.44E-06	1.52E-05	3.98E-06
525.25	550.25	1.74E-05	2.54E-06	2.08E-05	3.71E-06	1.35E-05	3.30E-06
550.25	575.25	1.59E-05	2.74E-06	1.26E-05	3.99E-06	1.21E-05	3.56E-06
575.25	600.25	1.10E-05	3.00E-06	1.27E-05	4.35E-06	2.25E-05	3.87E-06
600.25	625.25	1.31E-05	2.76E-06	1.59E-05	4.05E-06	1.09E-05	3.62E-06
625.25	650.25	1.67E-05	2.73E-06	1.01E-05	4.00E-06	1.56E-05	3.56E-06
650.25	680.25	8.97E-06	2.69E-06	-1.5E-06	3.69E-06	6.33E-06	3.32E-06
680.25	720.25	6.82E-06	2.68E-06	7.88E-06	3.91E-06	4.68E-06	3.56E-06
720.25	770.25	1.06E-05	2.10E-06	3.79E-06	2.96E-06	7.30E-06	2.64E-06
770.25	830.25	8.54E-06	2.03E-06	1.20E-05	2.92E-06	4.80E-06	2.60E-06
830.25	900.25	3.29E-06	1.97E-06	9.23E-06	2.89E-06	5.17E-06	2.58E-06
900.25	1000.25	6.97E-06	1.41E-06	4.36E-06	2.02E-06	4.36E-06	1.80E-06
1000.25	1300.25	3.61E-06	8.02E-07	1.50E-06	1.19E-06	3.43E-06	1.06E-06
1300.25	1700.25	2.16E-06	5.59E-07	1.63E-06	8.28E-07	2.30E-06	7.40E-07
1700.25	2200.25	1.26E-06	4.44E-07	5.08E-07	6.61E-07	1.38E-08	5.88E-07
2200.25	2800.25	5.32E-07	3.08E-07	6.37E-07	4.71E-07	1.40E-06	4.21E-07
2800.25	3500.25	1.17E-07	2.23E-07	9.57E-07	3.41E-07	8.72E-07	3.05E-07
3500.25	4300.25	4.27E-07	1.76E-07	6.15E-07	2.69E-07	4.48E-07	2.42E-07
4300.25	5200.25	2.82E-07	1.47E-07	1.65E-07	2.27E-07	1.01E-07	2.05E-07

